American Mineralogist, Volume 79, pages 289–301, 1994

Cation partitioning and substitution mechanisms in 1*M* phlogopite: A crystal chemical study

Giuseppe Cruciani, Pier Francesco Zanazzi
Dipartimento di Scienze della Terra, Università di Perugia, I-06100 Perugia, Italy

Abstract

The crystal chemistry of 1*M* phlogopite was studied by single-crystal X-ray diffraction and microprobe analysis. Structural refinement was carried out in space group *C*2/*m* (*R* values between 0.021 and 0.052) on 24 samples from basic lamproites, leucitites, kimberlite, and carbonatites.

The geometric and chemical features of the octahedral sites show the preferential partitioning of high-charge cations (Ti^{4+}, Al^{3+}, Cr^{3+}, Fe^{3+}) in the cis M2 sites. Bond-length and edge-length distortion parameters show the remarkably different behavior of the two octahedral sites when the high-charge cation content increases. The external shape of the trans M1 polyhedron is heavily constrained by the average field strength in the M2 sites.

In Ti-rich phlogopite the central cations of M2 sites show a significant off-center shift toward the O4 position. The substitution mechanism $^{[6]}(R^{2+}) + 2(OH)^- = {}^{[6]}(Ti^{4+}) + 2O^{2-}$ best explains the observed structural modifications. The loss of a proton linked to O4 is mainly recognized from the shortening of the *c* lattice dimension.

The consequences of octahedral cation partitioning and structural adjustments related to the Ti substitution may be important when dealing with the thermal stability field of phlogopite and mica-based geothermometry or geobarometry and can help in understanding the dependence of Ti solubility on temperature, f_{O_2}, and a_{H_2O}.

Introduction

Trioctahedral micas along the phlogopite-annite join occur as rock-forming minerals over a wide range of petrogenetic environments. Much systematic chemical study has been devoted to evaluating the most effective substitution mechanisms on both natural and synthetic micas. Some problems of the crystal chemical modeling of micas arise from the chemical substitution of high-charge cations for Mg^{2+} and Fe^{2+}. As these cations are probably nonrandomly distributed over the sixfold-coordinated sites, this implies that a complete description of the population of each site is possible only by assuming a reliable cation ordering model. As discussed recently by Guidotti and Dyar (1991), some simplifications to the site substitution schemes used in formulating the solution and activity models may greatly affect conclusions from geothermometric and geobarometric studies.

Different cation ordering patterns for the end-member micas have been extensively investigated by means of single-crystal X-ray diffraction. The basic geometric features of the various arrangements and relative stabilities are discussed and reviewed in Toraya (1981), Bailey (1984), Guggenheim (1984), and Guggenheim and Eggleton (1987).

This work is a systematic investigation of 1*M* natural rock-forming Mg-rich micas (phlogopite *sensu lato*) by means of single-crystal X-ray diffraction and microprobe analysis. The aim is to estimate to what extent high-charge cations can control ordering mechanisms within the octahedral layer. The octahedral cation partitioning model based on the normal ordering scheme (Bailey, 1984; Guggenheim, 1984) was analyzed, not only to check the validity of the model, but also to obtain a complete description of the population of each octahedral site. This study was performed over a large, although not fully representative, selection of phlogopite forming in a variety of physical and chemical conditions; special interest was devoted to some samples of igneous Mg-rich micas from rocks believed to have formed in the upper mantle.

Ti may be considered representative of the high field strength elements, and its geochemical behavior in phlogopite has been extensively studied by experimental petrologists. The occurrence of three main Ti substitution mechanisms (Ti □, Ti-Tschermak's, and Ti-oxy) has been proposed and discussed by several authors. Bohlen et al. (1980), Dymek (1983), and Bol et al. (1989) suggested that the loss of proton in micas is a valid mechanism for maintaining the charge balance when bivalent cations are replaced by tri- or tetravalent cations, but the oxy-component is commonly neglected because of the analytical uncertainties in the Fe^{3+} and OH contents. As shown by Hewitt and Abrecht (1986) and Abrecht and Hewitt (1988), evidence for Ti-oxy substitution based only upon chemical analyses may be ambiguous, even when data on Fe^{3+} and OH contents are available. In this work we analyze the structural indications for the occurrence of Ti-oxy substitution in phlogopite.

0003–004X/94/0304–0289$02.00

Table 1. Description of mica samples

Sample	Host rock	Locality	Reference
1	Leucocratic dike in garnet lherzolite	La Gallega (Ronda, Spain)	Gervilla and Leblanc (1990)
2	Nodule in carbonatite	Polino (Umbria, Italy)	Stoppa and Lavecchia (1992)
3	Pegmatitic vein in olivine melilitite	S. Venanzo (Umbria, Italy)	Cundari and Ferguson (1991)
4, 5	Ejecta in ultrapotassic pyroclastic rock	Albani Hills (Latium, Italy)	Gianfagna and Tuzi (1988)
6	Lamproite	Cabezo María (Vera, Spain)	Fuster (1956)
7	Kalsilitite	Cupaello (Latium, Italy)	Cundari and Ferguson (1991)
8	Ultramafic xenolith in lamproite	Torre Alfina (Latium, Italy)	Conticelli and Peccerillo (1990)
9	Ejecta with mica + cpx + ol	Vesuvio (Campania, Italy)	Di Girolamo (personal communication)
10	Leucititic tephrite	Albani Hills (Latium, Italy)	Dolfi (personal communication)
11	Phlogopitic clinopyroxenite nodule	Roccamonfina (Campania, Italy)	Giannetti and Luhr (1990)
12	Pyroclastic rock with sanidine	Acquasparta (Umbria, Italy)	Stoppa and Lavecchia (1992)
14	Lamproite	Torre Alfina (Latium, Italy)	Conticelli and Peccerillo (1990)
15	Metagabbro	Priestley Glacier (Antarctica)	Lombardo et al. (1987)
16	Nepheline melilitite	Eifel (Germany)	Keller and Schleicher (1990)
17, 19	Kimberlite	Finsch Pipe (South Africa)	Fraser and Hawkesworth (1992)
18	Lamproite	S.E. Yugoslavia	Holl (1990), Holl and Altherr (1991)
21–23	Leucitite	Begargo Hill (N.S.W., Australia)	Cundari (1973)
24	Carbonatite (sövite)	Araxà (Minas Gerais, Brazil)	da Silva et al. (1979)
25	Carbonatite (sövite)	Araxà (Minas Gerais, Brazil)	da Silva et al. (1979)
26	Carbonatite	Fort Portal (Uganda, Africa)	Barker and Nixon (1989)

Note: samples suppliers (sample no.): F. Gervilla (University of Granada, Spain) (1); F. Stoppa (University of Perugia, Italy) (2, 3, 7, 8, 12, 14, 16); A. Gianfagna (University of Rome, Italy) (4, 5); collected by G.C. (6); P. Di Girolamo (University of Naples, Italy) (9); D. Dolfi (University of Rome, Italy) (10); B. Giannetti (University of Rome, Italy) (11); B. Lombardo (University of Turin, Italy) and F. Talarico (University of Siena, Italy) (15); A. Cundari (University of Melbourne, Australia) (17, 19, 21, 22, 23); A. Holl and R. Altherr (University of Karlsruhe, Germany) (18); P. Comin-Chiaramonti (University of Palermo, Italy) (24, 25); D.S. Barker (University of Austin, Texas) (26).

Experimental

Sample description

The 24 specimens of mica used in this study are tabulated in Table 1. The geological and petrological setting is well characterized for most of the host rocks. Given references provide specific information on mineral assemblages and other petrological details.

X-ray structural study

Several mica crystals from each rock specimen were carefully hand-picked from crushed material. Only crystals with sharp optical extinction were considered suitable for the diffraction measurements.

Zero-level and first-level Weissenberg photographs were taken on crystals, mounted along the **a** axis, to evaluate the crystal mosaic structure and periodicity of stacking along **c***. The distribution of intensities along rows 13*l* and 02*l* was studied to determine polytypes according to Bailey (1988). All crystals analyzed on the diffractometer for data collection were 1*M* polytypes (space group *C*2/*m*), although 3*T* and $2M_1$ polytypes were also found in samples from lamproites.

Intensity data were collected on a Philips PW1100 four-

Table 2. Crystallographic data and cell parameters for 1*M* phlogopite samples

Sample	Dimensions (mm)	No. tot. refl.	No. obs. refl.	*R*	*a*	*b*	*c*	β
1	0.51 × 0.21 × 0.03	724	613	2.3	5.325(1)	9.236(1)	10.242(2)	100.12(2)
2	0.18 × 0.15 × 0.02	632	517	2.7	5.313(1)	9.210(1)	10.286(2)	99.91(2)
3	0.19 × 0.14 × 0.02	659	507	2.4	5.321(1)	9.219(1)	10.124(2)	100.15(2)
4	0.18 × 0.12 × 0.04	585	464	2.7	5.327(1)	9.228(1)	10.217(2)	100.05(2)
5	0.26 × 0.12 × 0.04	689	549	2.4	5.324(1)	9.217(1)	10.230(2)	100.04(2)
6	0.18 × 0.11 × 0.03	570	371	4.3	5.316(1)	9.202(2)	10.212(4)	100.12(3)
7	0.16 × 0.12 × 0.03	649	437	3.5	5.310(1)	9.200(2)	10.277(2)	99.92(2)
8	0.16 × 0.14 × 0.03	525	325	3.6	5.315(1)	9.200(2)	10.193(3)	100.01(3)
9	0.25 × 0.22 × 0.03	699	585	2.3	5.317(1)	9.211(2)	10.228(2)	100.01(2)
10	0.20 × 0.13 × 0.03	668	514	2.5	5.319(1)	9.217(1)	10.208(2)	100.03(2)
11	0.22 × 0.11 × 0.04	678	557	2.2	5.319(1)	9.212(1)	10.251(2)	100.04(2)
12	0.26 × 0.15 × 0.02	655	466	2.7	5.330(1)	9.229(1)	10.196(2)	100.06(2)
14	0.27 × 0.16 × 0.02	668	363	5.2	5.320(2)	9.218(3)	10.217(2)	100.11(2)
15	0.20 × 0.15 × 0.02	607	372	3.7	5.335(1)	9.242(2)	10.202(3)	100.05(3)
16	0.26 × 0.20 × 0.03	704	472	4.7	5.322(8)	9.223(9)	10.190(5)	100.02(4)
17	0.19 × 0.17 × 0.04	677	504	2.7	5.334(1)	9.240(2)	10.225(4)	100.06(3)
18	0.28 × 0.25 × 0.03	686	529	2.6	5.314(1)	9.204(1)	10.182(1)	100.03(1)
19	0.20 × 0.16 × 0.03	625	410	4.4	5.338(1)	9.244(1)	10.259(2)	100.12(2)
21	0.29 × 0.26 × 0.04	706	579	2.1	5.336(1)	9.244(1)	10.089(2)	100.29(2)
22	0.18 × 0.13 × 0.03	546	414	3.5	5.336(2)	9.245(2)	10.079(5)	100.30(4)
23	0.16 × 0.15 × 0.04	661	558	2.6	5.337(1)	9.249(1)	10.096(3)	100.31(3)
24	0.20 × 0.16 × 0.04	668	409	3.2	5.339(1)	9.251(2)	10.298(3)	99.86(3)
25	0.16 × 0.12 × 0.04	653	416	3.3	5.337(1)	9.243(2)	10.298(3)	99.92(3)
26	0.21 × 0.18 × 0.04	675	526	2.7	5.331(1)	9.228(2)	10.240(3)	100.02(3)

Note: $R = \Sigma (||F_o| - |F_c||)/\Sigma F_o \times 100$. Lengths in ångströms, angles in degrees. Estimated standard deviations in parentheses refer to the last digit.

circle automated diffractometer using graphite-monochromatized Mo$K\alpha$ radiation. Unit-cell parameters were refined by the least-squares method applied to fit the setting angles of 25 reflections in the range $8° \leq \theta \leq 15°$. For each crystal, the equivalent hkl and $h\bar{k}l$ pairs were measured in the θ range 2–30°, using the ω scan mode (speed scan of 1°/min, 3–5° width, and time of 20 s on backgrounds). Data were corrected for Lorentz and polarization factors. Absorption correction was applied according to the semiempirical method of North et al. (1968). Only reflections in which $I > 3\sigma(I)$ [in a few cases $I > 5\sigma(I)$] were employed for the least-squares refinement of each sample.

Least-squares refinement was carried out in space group $C2/m$ starting from the atomic coordinates of the end-member phlogopite (Hazen and Burnham, 1973). The full matrix program of the SHELX-76 crystallographic package was used for computation (Sheldrick, 1976). Neutral atomic scattering factors were used (Ibers and Hamilton, 1974). Fe and Mg scattering curves, with the constraint that $X_{(Mg)} + X_{(Fe)} = 1$, were used to fit the experimental electron density in the octahedral sites. Anisotropic displacement parameters and occupancy were refined in alternate cycles. In general, the composition of the tetrahedral site was fixed as 0.75 Si and 0.25 Al. Only for samples 17 and 19 (from kimberlite) and samples 24 and 25 (from carbonatite) was it possible to refine the occupancy factors of Si vs. Fe within the tetrahedra. Refinements converged to R values in the range 0.021–0.052 (mean 0.031). Unit-cell parameters and some details regarding data collection and refinement procedure are given in Table 2. Final atomic coordinates and temperature parameters are listed in Table 3[1]; the atomic labeling is the same as in Hazen and Burnham (1973). Observed and calculated structure amplitudes are reported in Table 4[1]; selected interatomic bond distances and site volumes are shown in Table 5.[1] Table 6 contains some other structural parameters describing the geometry of the mica layer. The electron densities of the cation sites, as obtained from the refinement of the occupancy factors, are given in Table 7 and are compared with those calculated from microprobe analyses.

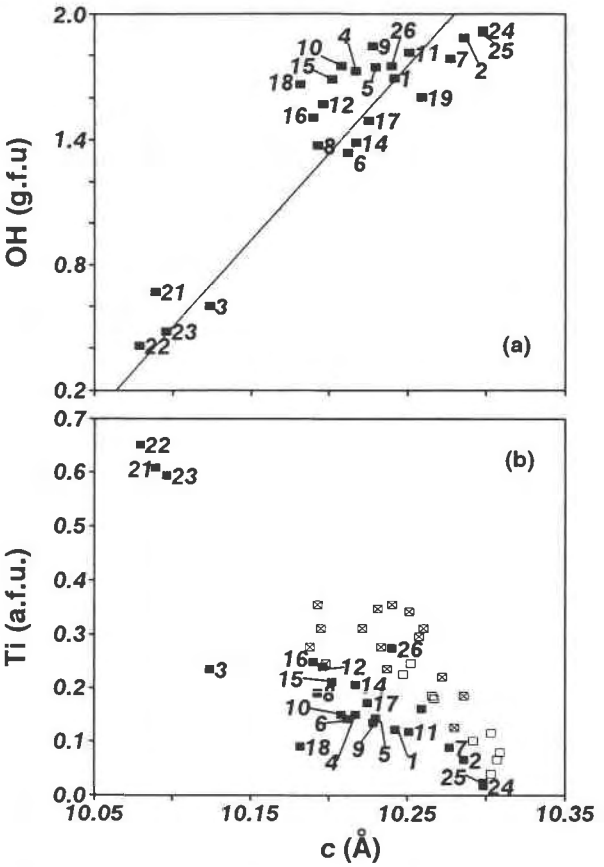

Fig. 1. (**a**) Plot of c lattice parameter vs. estimated OH content, expressed as OH groups per formula unit (g.f.u.). Line refers to the equation $OH = 8.3(9) \cdot c - 83.7(1)$, $R^2 = 0.88$, by regression analysis on data from Brigatti and Davoli (1990) and Brigatti et al. (1991). (**b**) Plot of c parameter vs. $^{[6]}$Ti content (a.f.u. = atoms per formula unit). Solid symbols are for micas in this work; open symbols refer to data from Tables 2 and 3 of Abrecht and Hewitt (1988) on Mg-rich synthetic micas (boxes) and Fe-rich synthetic micas (boxes with crosses).

Microprobe analyses

Quantitative chemical analyses were acquired from the same crystals used for structural refinements (except for sample 3, where analyses were taken from six other crystals from the same rock). Samples were analyzed on a Cameca Camebax microprobe operating in WDS. Working conditions were those employed by Foley (1990) on lamproitic phlogopite using similar equipment. Four to six point analyses were taken for each crystal and averaged. The amount of Li was analyzed on an ion microprobe.

For formula calculations, several normalization schemes were tried and compared. The first scheme (11 atoms) is based on a fixed number $[O_{10}(OH, F)_2]$ and 22 negative charges; in the second scheme the complete occupancy of octahedral and tetrahedral sites (seven cations) is assumed; the third scheme followed the iterative method of Dymek (1983), which is based on the assumption that only the (R^{3+}, R^{4+})-□ substitution occurs. It was found that each of these methods has severe limitations, depending on the specific assumption on which it is based. Both orders of preference $Ti > Fe^{3+}$ and $Fe^{3+} > Ti$ were assumed in filling the tetrahedral sites when the sum of Si + Al was <4 apfu, and the latter was chosen on the basis of the crystal chemical results. We finally adopted the following multistep procedure: (1) The normalization scheme using 11 O atoms was employed for the first calculation of the numbers of ions, and the method of Dy-

[1] A copy of Tables 3, 4, 5, and 9 may be ordered as Document AM-94-547 from the Business Office, Mineralogical Society of America, 1130 Seventeenth Street NW, Suite 330, Washington, DC 20036, U.S.A. Please remit $5.00 in advance for the microfiche.

TABLE 6. Structural parameters for the 1*M* phlogopite samples

	1	2	3	4	5	6	7	8	9	10	11
$^{[4]}t$	2.232	2.237	2.238	2.237	2.238	2.244	2.256	2.236	2.242	2.236	2.243
$^{[6]}t$	2.136	2.137	2.118	2.134	2.133	2.119	2.143	2.117	2.130	2.128	2.129
K-O4	3.955	3.991	3.928	3.956	3.959	3.969	3.973	3.955	3.962	3.959	3.970
ψ_{M1}	59.14	58.94	59.29	59.12	59.07	59.18	58.93	59.32	59.10	59.13	59.13
ψ_{M2}	58.92	58.89	59.11	58.94	58.96	59.10	58.75	59.06	58.96	59.00	58.96
τ	110.20	110.48	110.71	110.24	110.27	110.67	111.01	110.46	110.48	110.18	110.34
α	8.72	9.68	5.74	9.06	9.24	8.35	7.97	7.92	9.44	9.48	9.67
$\Delta_{K\text{-}O}$	0.398	0.441	0.265	0.413	0.419	0.377	0.361	0.360	0.429	0.432	0.440
D.M.	0.545	0.562	0.498	0.553	0.556	0.544	0.508	0.538	0.562	0.567	0.571
Δz	0.006	−0.003	0.001	0.010	0.004	−0.007	−0.007	0.016	0.003	0.005	0.003
M1-BLD	0.753	0.885	1.029	0.962	0.900	1.355	0.722	0.771	0.868	1.093	0.851
M1-ELD	5.285	5.047	5.458	5.267	5.209	5.344	5.041	5.491	5.236	5.282	5.284
M2-BLD	0.645	0.661	1.422	1.394	1.209	1.390	0.839	1.733	1.130	1.420	1.033
M2-ELD	4.207	4.148	4.392	4.188	4.184	4.301	4.030	4.320	4.201	4.197	4.211
M2-shift	−0.003	−0.010	0.013	0.021	0.016	0.019	0.005	0.031	0.012	0.023	0.011

Note: $^{[4]}t$ (Å): tetrahedral sheet thickness calculated from z coordinates of basal and apical O atoms; $^{[6]}t$ (Å): octahedral sheet thickness as defined by Hazen and Burnham, 1973; K-O4 (Å): projection of K-O4 distance along **c***; ψ_{M1} and ψ_{M2} (°): octahedral flattening angles (as in Hazen and Burnham, 1973); τ (°): tetrahedral flattening angle; α (°): tetrahedral rotation angle (as in Hazen and Burnham, 1973); $\Delta_{(K\text{-}O)}$ (Å): $\langle K\text{-}O_{outer}\rangle - \langle K\text{-}O_{inner}\rangle$; D.M. (Å): dimensional misfit between tetrahedral and octahedral sheets defined as D.M. = $[2\sqrt{3}\langle T\text{-}O_{bas}\rangle - 3\sqrt{2}\langle M\text{-}O\rangle]$ (Toraya, 1981); Δz (Å): departure from coplanarity of the basal O atoms, calculated as $\Delta z = (z_{O2} - z_{O1})c \sin\beta$ (modified from Hazen and Burnham, 1973); BLD and ELD: octahedral bond-length and edge-length distortion parameters as calculated by Kunz et al. (1991); M2-shift (Å): off-center shift of the M2 cation defined as the distance between the refined position of cation and the geometrical center of M2 site (coordinates: $x/a = 0.0$, $y/b = 0.8333$, $z/c = 0.5$). Positive values are for shifts toward the O4 site, and negative values are for shifts toward the O3 site. The estimated standard deviations on lengths and distortion parameters are <0.002.

mek (1983) was used for a rough evaluation of FeO/(FeO + Fe_2O_3) ratios. (2) A semiquantitative estimation of OH content was obtained from the c-cell parameter (Fig. 1a) by the equation OH = 8.3(9)·c − 83.7(1), R^2 = 0.88, which has been calculated by regression analysis from data from Brigatti and Davoli (1990) and Brigatti et al. (1991). Noda and Ushio (1965) found a similar equation for the OH ↔ F substitution in synthetic phlogopite. This relationship is explained by decreased coulombic repulsion between the proton and the interlayer cation in OH-poor micas (McCauley et al., 1973; Giese, 1984; Munoz, 1984). (3) Formulas were calculated again on the basis of the anionic charge inferred by $O_{12-x-y}OH_xF_y$. (4) The consistency and the accuracy of the calculations were evaluated by taking into account several well-defined relationships, involving structural parameters, observed in this study and from the literature. Best-fit calculations were achieved by trial and error. The complete description for the normalization procedure and discussion of results are reported in Cruciani (1993). Oxide percentages resulting from chemical analyses and numbers of ions calculated by the multistep procedure are given in Table 8.

DISCUSSION OF RESULTS

Variations of cell parameters with composition

In most samples the a and b cell dimensions are those imposed by the octahedral sheet, (a = 5.368(3) − X_{Mg}·6.3(6)·10^{-2}, R^2 = 0.85; b = 9.308(5) − X_{Mg}·12.1(9)·10^{-2}, R^2 = 0.91; N_{obs} = 20, X_{Mg} = Mg/$^{[6]}$total). Samples 17 and 19 (from the Finsch Pipe kimberlite) and 24 and 25 (from the Araxà carbonatite), with (Si + Al)$_{tot}$ < 4 apfu, have a and b parameters greater than those expected from their octahedral composition, suggesting stronger control by the tetrahedral sheet in which substitutions other than Si ↔ Al take place.

The shortening of c shows a significant relationship with the $^{[6]}$Ti content, as observed by Abrecht and Hewitt (1988) in synthetic phlogopite and biotite (Fig. 1b).

Tetrahedral site geometry

On average, individual tetrahedra are fairly regular and slightly elongated along the T-O_{apical} bond distance, a common feature in trisilicic micas. For most samples, the variation of tetrahedral mean bond lengths can be mod-

TABLE 7. Scattering power (electrons) in octahedral and interlayer cation sites

	1	2	3	4	5	6	7	8	9	10	11
M1 electrons	16.2(1)	12.8(1)	13.6(1)	15.7(1)	14.8(1)	12.7(1)	12.0(1)	13.0(2)	14.4(1)	15.2(1)	14.7(1)
M2 electrons	15.9(1)	12.8(1)	13.7(1)	15.6(1)	14.8(1)	13.1(2)	12.0(1)	13.8(3)	14.5(1)	15.3(1)	14.8(1)
$^{[6]}$electrons	48.0	38.4	40.9	46.9	44.5	38.9	36.1	40.6	43.4	45.8	44.2
$^{[6]}$EMPA	48.0	40.1	41.2	48.1	45.4	39.1	38.5	40.6	43.4	47.3	44.2
K electrons	17.4(1)	18.8(1)	20.1(1)	19.6(1)	18.9(1)	19.5(1)	22.1(1)	19.0(3)	18.5(1)	20.3(5)	18.6(1)
$^{[12]}$EMPA	17.2	18.2	19.2	19.1	17.7	18.3	18.6	18.1	17.9	19.3	17.5

Note: M1 electrons, M2 electrons, and K electrons are from X-ray refinements in M1, M2, and interlayer sites, respectively; estimated standard deviations refer to the last digit; $^{[6]}$electrons = M1 electrons + 2·M2 electrons; $^{[6]}$EMPA and $^{[12]}$EMPA are the electrons calculated from the chemical analysis for the octahedral and interlayer cations.

TABLE 6.—*Continued*

12	14	15	16	17	18	19	21	22	23	24	25	26
2.241	2.239	2.233	2.236	2.238	2.235	2.247	2.249	2.256	2.254	2.249	2.244	2.238
2.130	2.126	2.128	2.107	2.138	2.131	2.144	2.122	2.121	2.132	2.150	2.152	2.140
3.948	3.961	3.931	3.965	3.959	3.939	3.966	3.901	3.887	3.885	3.987	3.989	3.961
59.19	59.27	59.35	59.42	59.08	59.05	58.89	59.58	59.50	59.46	58.95	58.84	59.08
59.00	58.98	58.98	59.25	58.94	58.94	58.94	59.01	59.07	58.90	58.83	58.84	58.88
110.24	110.45	110.04	110.02	110.60	110.55	110.71	110.64	110.55	110.67	110.60	110.60	110.33
8.82	7.46	7.38	9.68	7.81	8.51	7.89	5.70	5.58	5.27	9.10	9.25	8.62
0.401	0.331	0.342	0.444	0.355	0.391	0.360	0.262	0.260	0.244	0.412	0.414	0.394
0.551	0.518	0.528	0.597	0.522	0.538	0.519	0.498	0.498	0.483	0.542	0.540	0.538
0.007	0.006	0.000	0.009	0.005	0.003	−0.001	0.020	0.026	0.018	0.002	0.000	0.007
1.010	0.913	0.670	1.336	0.849	0.805	0.811	1.193	1.261	0.906	0.672	0.881	0.849
5.358	5.425	5.529	5.620	5.229	5.167	5.003	5.803	5.712	5.661	5.072	4.936	5.215
1.725	1.600	0.872	2.248	1.287	1.082	1.099	2.960	2.795	2.632	0.658	0.641	1.610
4.218	4.247	4.259	4.398	4.202	4.211	4.242	4.195	4.210	4.095	4.137	4.096	4.129
0.037	0.026	0.016	0.057	0.014	0.010	0.011	0.083	0.087	0.079	−0.010	−0.010	0.033

eled as a linear combination of the ⟨Al-O⟩ and ⟨Si-O⟩ bond distances on the basis of the chemical data (Cruciani, 1993). The enlargement of the tetrahedra of samples 17, 19, 24, and 25 implies the presence of a cation larger than Al. These samples have sums of Si + Al < 4 apfu, and reverse pleochroism, suggesting $^{[4]}Fe^{3+}$. The occurrence of $^{[4]}Fe^{3+}$ in sample 24 was confirmed by means of X-ray absorption spectroscopy (XANES) (Cruciani and Quartieri, 1992). A detailed description of single-crystal X-ray characterization of those phlogopite samples is given elsewhere (Cruciani and Zanazzi, 1992).

Tetrahedral sheet and interlayer site geometry

Tetrahedral rotation (α) (Newnham and Brindley, 1956; as in Hazen and Burnham, 1973) and out-of-plane tilting of basal O atoms (i.e., basal corrugation, Δz (Güven, 1971) are the most common parameters for describing interpolyhedral geometry in the tetrahedral sheet and the ditrigonality of the interlayer site. A close linear relationship exists between the tetrahedral rotation and the difference $\Delta_{(K\text{-}O)} = \langle K\text{-}O_{outer}\rangle - \langle K\text{-}O_{inner}\rangle$ (McCauley and Newnham, 1971). For the studied micas, linear regression yields $\Delta_{(K\text{-}O)} = 0.009(3) + \alpha 4.5(5)\cdot 10^{-3}$; $N_{obs} = 24$, $R^2 = 0.997$. As discussed by several authors (see Bailey, 1984, for a review) the in-plane rotation of adjacent tetrahedra is generally the most effective mechanism for the fitting of the lateral dimensions of the tetrahedral and octahedral sheets. This is confirmed by the positive trend between the tetrahedral rotation and the dimensional misfit parameters (Fig. 2). The dimensional misfit is a function of the chemical composition of octahedral and tetrahedral sheets. Mg-rich micas generally have higher α, $\Delta_{K\text{-}O}$, and D.M. values (as defined in Table 2) than Fe-rich micas. The occurrence of some Mg-rich micas in a field of low α-$\Delta_{(K\text{-}O)}$ values may be explained by their high F content. In Figure 3, the increase in the estimated OH content is accompanied by a significant increase in the longer mean K-O bond distance ($\langle K\text{-}O_{outer}\rangle$) and by a very slight decrease in the shorter mean K-O bond distance ($\langle K\text{-}O_{inner}\rangle$), resulting in a greater difference $\Delta_{(K\text{-}O)}$. The substitution (F, O) ↔ OH on O4 may be associated with bond length variations of the interlayer site on the basis of the weak electrostatic interactions between the H and the O atoms of the interlayer site. Guggenheim et al. (1987) concluded that the proton in muscovite is able to weaken (lengthen) the longer K-O bonds with respect to the others. In phlogopite, the loss of H may be a complementary explanation, together with the decrease in the dimensional misfit, for the increased regularity of the interlayer cavity. The above consideration is also in agreement with the $\Delta_{(K\text{-}O)}$ values found for the oxybiotite (Ohta et al., 1982), which are smaller than those for the hydrogenated sample (Takeda and Ross, 1975). Samples featured by the lowest α, $\Delta_{(K\text{-}O)}$, and D.M. values also have relatively high Ba content, which can be favored by or responsible for a decreased ditrigonality. Further discussion on this point is given in a later section on the basis of the bond valence theory.

The corrugation of basal O atoms, Δz, has positive and negative values, depending on the different ways the tet-

TABLE 7.—*Continued*

12	14	15	16	17	18	19	21	22	23	24	25	26
15.1(1)	13.6(2)	16.6(1)	13.6(1)	13.1(1)	13.5(1)	13.3(2)	16.9(1)	16.7(1)	17.0(1)	12.8(1)	12.7(1)	14.8(1)
15.2(1)	14.3(3)	16.7(1)	14.9(2)	13.2(1)	13.8(1)	13.5(3)	17.1(1)	17.5(2)	17.1(1)	12.7(1)	12.6(1)	15.2(1)
45.5	42.1	50.0	43.3	39.5	41.0	40.4	51.0	51.6	51.2	38.3	38.0	45.2
47.7	41.5	48.3	44.8	40.6	40.5	41.2	51.0	51.5	51.2	38.4	37.9	45.2
19.6(1)	18.5(3)	17.5(2)	19.1(1)	18.9(1)	18.5(1)	19.0(1)	23.5(1)	25.6(1)	23.2(1)	18.0(2)	17.8(2)	18.0(1)
18.7	18.0	17.1	18.6	19.1	17.9	17.7	23.5	23.9	24.7	17.5	17.6	18.7

TABLE 8. Microprobe analyses of mica samples

	1	2	3	4	5	6	7	8	9	10	11
SiO_2	36.72	38.48	40.25	35.98	37.41	39.92	40.54	38.23	37.07	35.30	36.97
Al_2O_3	16.82	15.79	11.28	15.95	15.79	12.59	12.56	13.13	15.96	15.98	16.74
MgO	14.39	23.75	19.38	16.13	19.46	23.15	24.64	22.84	21.68	18.40	19.77
FeO	12.41	3.17	8.45	12.92	9.49	3.18	2.91	4.12	6.71	10.98	8.01
TiO_2	2.11	1.21	4.28	2.64	2.60	2.60	1.63	3.44	2.43	2.64	2.12
Cr_2O_3	0.00	1.27	0.01	0.05	0.21	1.38	0.34	1.20	0.22	0.01	0.09
MnO	0.09	0.01	0.16	0.14	0.10	0.01	0.00	0.01	0.04	0.11	0.06
Li_2O	0.012	0.001	0.018	n.d.	n.d.	0.004	0.008	0.002	0.000	n.d.	n.d.
K_2O	9.08	10.25	9.79	9.50	9.36	10.22	10.61	10.02	9.28	9.31	9.40
Na_2O	0.17	0.04	0.20	0.14	0.27	0.20	0.06	0.13	0.51	0.17	0.24
BaO	0.00	0.08	1.06	0.90	0.43	0.04	0.01	0.07	0.41	1.23	0.18
CaO	0.00	0.07	0.00	0.01	0.00	0.00	0.00	0.00	0.00	0.01	0.01
F	0.28	0.52	6.10	0.74	0.68	2.90	0.97	1.85	0.47	0.81	0.38
Total	92.08	94.62	100.97	95.09	95.82	96.18	94.27	95.02	94.78	94.97	93.95
$-O = F$	0.12	0.22	2.57	0.31	0.29	1.22	0.41	0.78	0.20	0.34	0.16
Number of ions on the basis of 12 (O, OH, F)											
Si	2.826	2.768	2.926	2.708	2.735	2.891	2.922	2.817	2.707	2.660	2.729
$^{[4]}Al$	1.174	1.232	0.967	1.292	1.265	1.075	1.067	1.140	1.293	1.340	1.271
$^{[4]}Fe^{3+}$	0.000	0.000	0.107	0.000	0.000	0.034	0.011	0.043	0.000	0.000	0.000
$^{[6]}Al$	0.352	0.107	0.000	0.123	0.096	0.000	0.000	0.000	0.080	0.080	0.186
Mg	1.651	2.546	2.100	1.810	2.120	2.499	2.648	2.509	2.360	2.067	2.175
Fe^{2+}	0.759	0.191	0.308	0.651	0.464	0.145	0.105	0.203	0.389	0.657	0.445
Fe^{3+}	0.040	0.000	0.100	0.163	0.117	0.014	0.059	0.008	0.021	0.035	0.050
Ti	0.122	0.065	0.234	0.149	0.143	0.142	0.089	0.190	0.134	0.150	0.118
Cr	0.000	0.072	0.000	0.003	0.012	0.079	0.019	0.070	0.013	0.001	0.005
Mn	0.006	0.000	0.010	0.009	0.006	0.000	0.000	0.000	0.003	0.007	0.004
Li	0.004	0.000	0.005	—	—	0.001	0.002	0.001	0.000	—	—
$^{[6]}$Total	2.934	2.981	2.757	2.908	2.958	2.880	2.920	2.981	3.000	2.997	2.983
K	0.891	0.941	0.908	0.912	0.873	0.944	0.975	0.942	0.864	0.895	0.885
Na	0.025	0.005	0.028	0.020	0.039	0.028	0.008	0.018	0.072	0.025	0.034
Ba	0.000	0.002	0.030	0.027	0.012	0.001	0.000	0.002	0.012	0.036	0.005
Ca	0.000	0.005	0.000	0.000	0.000	0.000	0.000	0.000	0.000	0.001	0.000
$^{[12]}$Total	0.916	0.953	0.966	0.959	0.924	0.973	0.983	0.962	0.948	0.957	0.924
F	0.068	0.118	1.402	0.175	0.158	0.665	0.221	0.431	0.109	0.194	0.088
OH	1.692	1.882	0.598	1.725	1.742	1.335	1.779	1.369	1.846	1.746	1.812

Note: number of ions calculated by the multistep procedure. OH contents estimated from the relationship with *c* lattice parameter.

rahedra tilt, which are in turn linked to the movement of the apical O. Enlargement of the M1 site with respect to the M2 sites causes a shift of the apical O, which is consistent with $\Delta(z) > 0$, a common finding for most of our samples.

Octahedral site geometry

For all studied micas, the volumes and flattening angles of the trans M1 octahedral site are larger than those of the cis M2 site. These features can be referred to as the so-called normal ordering scheme, as defined by Bailey (1984) and Guggenheim (1984).

The normal ordering scheme has been described as an arrangement in which enlargement of the M1 site with respect to the M2 site and partitioning of high-charge, small-radius cations within the M2 site are favored by geometric and energy factors (Radoslovich, 1963; Toraya, 1981; Guggenheim, 1984; Guggenheim and Eggleton, 1987). Furthermore, the large size of the M1 site and the constraint of local charge balance agree with octahedral vacancies in M1. This kind of cation ordering pattern has been experimentally found for several mica structures (Lin and Guggenheim, 1983; Ohta et al., 1982, and references therein).

To characterize the distortion of M1 and M2, bond-length and edge-length distortion (BLD and ELD) parameters (Renner and Lehmann, 1986; Kunz et al., 1991) were calculated. These parameters describe both the geometry of the octahedron (ELD) and the arrangement of the cation within it (BLD), i.e., the external distortion of polyhedra and displacement of the central atom from the geometrical center of the polyhedron.

The ELD values of the M1 site are higher than those of the M2 site. This is consistent with the greater flattening angles and angle variance of the M1 site. The BLD values are generally lower for M1 than for M2. These observations are in good agreement with those of Renner and Lehmann (1986) and Kunz et al. (1991): the smaller polyhedra appear to have relatively more distorted bond lengths and fewer distorted edge lengths.

The magnitude of the BLD parameter of the M2 site shows a clear increase with increasing $^{[6]}$Ti content, whereas the BLD of the M1 site is quite constant (Fig. 4). The high bond-length distortion of the M2 sites is also recognized by comparison of the individual M2-O bond distances: M2-OH and M2-O3 bond lengths show the prevalent displacement of the M2 cation from the geometric center of the octahedra toward O4, along the two-fold axis. This off-center shift in M2 is correlated with Ti content (Fig. 5). The off-center shift of Ti atoms within octahedra is well known for a wide group of Ti-rich compounds (Kunz et al., 1991, and references therein); it is

TABLE 8.—*Continued*

12	14	15	16	17	18	19	21	22	23	24	25	26
35.18	39.31	37.35	36.10	40.14	39.17	40.10	34.49	34.39	34.31	40.80	40.28	37.13
15.58	13.43	15.11	16.35	9.30	13.99	9.40	13.45	13.24	13.01	6.84	7.87	14.90
16.51	21.21	15.16	18.98	23.24	23.13	23.45	12.63	12.85	13.09	25.96	26.30	18.72
11.66	4.87	12.86	6.91	8.08	4.30	8.15	11.57	11.03	11.79	9.71	8.35	8.22
4.20	3.73	3.74	4.39	3.12	1.63	2.91	10.20	10.85	9.88	0.32	0.43	4.91
0.01	0.92	0.27	0.13	0.08	0.31	0.04	0.02	0.00	0.00	0.01	0.06	0.30
0.10	0.03	0.07	0.06	0.08	0.03	0.08	0.07	0.09	0.04	0.07	0.09	0.05
n.d.	0.002	0.017	0.000	0.001	0.002	0.001	0.017	0.017	0.017	0.003	0.003	n.d.
9.15	10.01	9.28	9.82	10.13	9.39	9.38	6.33	6.19	6.47	9.50	9.54	9.88
0.27	0.12	0.15	0.12	0.11	0.54	0.09	0.82	0.89	0.96	0.36	0.38	0.40
0.84	0.07	0.02	0.29	0.59	0.26	0.51	5.77	5.95	6.01	0.10	0.09	0.15
0.02	0.01	0.01	0.04	0.00	0.00	0.00	0.00	0.01	0.00	0.01	0.01	0.04
0.99	1.81	0.49	0.41	1.36	1.03	0.87	1.33	1.55	1.67	0.36	0.41	0.23
94.51	95.52	94.51	93.59	96.22	93.78	94.98	96.69	97.04	97.22	94.03	93.81	94.94
0.42	0.76	0.21	0.17	0.57	0.43	0.37	0.56	0.65	0.70	0.15	0.17	0.10
Number of ions on the basis of 12 (O, OH, F)												
2.664	2.880	2.802	2.717	2.940	2.864	2.945	2.730	2.741	2.736	2.974	2.930	2.749
1.336	1.120	1.198	1.283	0.803	1.136	0.814	1.255	1.244	1.223	0.588	0.675	1.251
0.000	0.000	0.000	0.000	0.257	0.000	0.241	0.015	0.015	0.041	0.438	0.395	0.000
0.054	0.039	0.138	0.168	0.000	0.070	0.000	0.000	0.000	0.000	0.000	0.000	0.049
1.863	2.316	1.695	2.130	2.537	2.520	2.566	1.490	1.527	1.556	2.820	2.853	2.066
0.517	0.269	0.645	0.391	0.237	0.184	0.240	0.536	0.514	0.550	0.107	0.043	0.509
0.223	0.030	0.162	0.044	0.002	0.079	0.021	0.216	0.207	0.196	0.050	0.072	0.000
0.239	0.205	0.211	0.248	0.172	0.090	0.161	0.607	0.650	0.592	0.017	0.023	0.273
0.001	0.053	0.016	0.007	0.005	0.018	0.002	0.001	0.000	0.000	0.001	0.003	0.017
0.006	0.002	0.004	0.004	0.005	0.002	0.005	0.005	0.006	0.003	0.004	0.005	0.003
—	0.001	0.005	0.000	0.000	0.000	0.000	0.005	0.006	0.006	0.001	0.001	—
2.903	2.915	2.876	2.992	2.958	2.963	2.995	2.860	2.910	2.903	3.000	3.000	2.917
0.884	0.935	0.888	0.943	0.946	0.876	0.879	0.639	0.629	0.658	0.883	0.886	0.933
0.040	0.017	0.021	0.017	0.016	0.076	0.013	0.125	0.137	0.148	0.050	0.054	0.058
0.025	0.002	0.000	0.008	0.017	0.008	0.015	0.179	0.186	0.188	0.003	0.003	0.004
0.002	0.001	0.001	0.003	0.000	0.000	0.000	0.000	0.001	0.000	0.001	0.001	0.003
0.951	0.955	0.910	0.971	0.979	0.960	0.907	0.943	0.953	0.994	0.937	0.944	0.998
0.238	0.419	0.116	0.098	0.314	0.238	0.203	0.333	0.390	0.421	0.083	0.094	0.054
1.562	1.381	1.684	1.502	1.486	1.662	1.597	0.667	0.410	0.479	1.917	1.906	1.746

noteworthy that this kind of distortion may occur even in cases of relatively low Ti content (e.g., micas). A similar feature has also recently been observed in amphiboles (Oberti et al., 1992).

The magnitude of ELD values for M1 shows a fairly good positive relationship with Ti content, although there is no relation between Ti and ELD values for M2 (Fig. 6).

Such different behavior of the internal and the external distortions between the M1 and M2 can be ascribed to the preference of Ti for M2. The correlation between the values of ELD for M1 and BLD for M2 and the Ti content may be understood by considering the geometric constraints within the mica octahedral sheet. When high-charge cations are partitioned into six smaller M2 octahedra surrounding one larger M1 site, the external distortion of the M1 polyhedron is expected to be strongly controlled. Lin and Guggenheim (1983) observed that the flattening of each octahedron is mainly dependent on the sum of the field strengths of the neighboring sites. Weiss et al. (1985) also deduced that the distortions in any particular octahedron are due to interaction in the whole sheet rather than in the octahedron alone. Consequently the increase in Ti on M2 may be responsible for external polyhedral distortions (ELD) of the isolated M1 polyhedron more than the effect exerted by the mean charge of the M1 site. This distortion behavior of the M1 and M2 sites was misinterpreted by Brigatti et al. (1991) as an indication of Ti preferential partitioning on M1.

Least-squares analysis

A least-squares program was constructed to merge the information obtained from the X-ray structural study and chemical analysis. The aim was to have a reliable quantitative description of the population of each octahedral site and to evaluate the consistency of the observed X-ray diffraction and chemical data with the cation partitioning model. A system of eight equations relating the experimental data was developed according to the following assumptions: (1) all high-charge, small-radius cations (Ti^{4+}, Al^{3+}, Cr^{3+}, Fe^{3+}) are located on M2; (2) full occupancy is assumed for the M2 site, whereas octahedral vacancies are considered on M1; (3) modeling of the observed mean bond lengths, as commonly found in the literature, is carried out by a linear combination of the ideal cation to O bond distances of the type: $\langle M\text{-}O\rangle = \Sigma\, x_n D_{id}$, where x_n is the fraction of the nth cation. The D_{id} ideal distances used here and listed below were taken from Weiss et al. (1992); only the $\langle Mg\text{-}O\rangle$ value, closer to the distance found by Hazen and Burnham (1973) for the

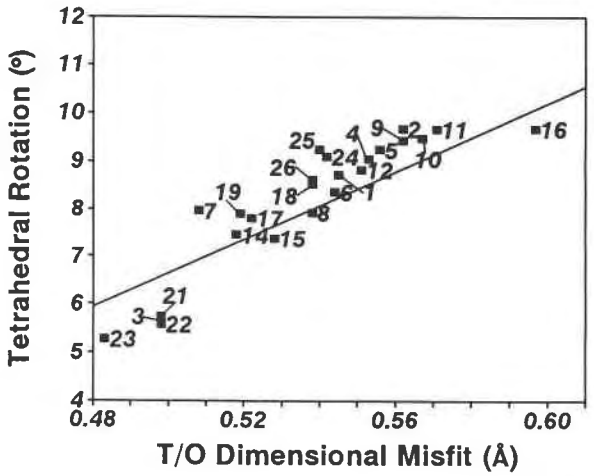

Fig. 2. Variation of tetrahedral rotation (α) vs. dimensional misfit (D.M.) between tetrahedral and octahedral sheets. Straight line represents the equation (α) = 35.44 (D.M.) − 11.09, reported by Toraya (1981).

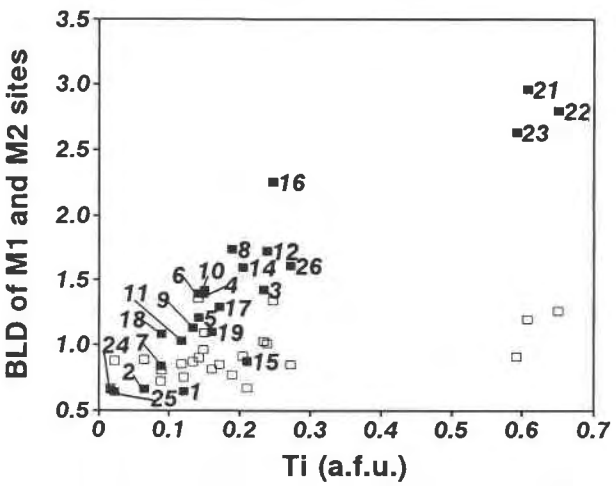

Fig. 4. Plot of bond-length distortion parameter of octahedral sites M1 (open symbols and labels) and M2 (solid symbols) vs. [6]Ti content.

end-member phlogopite, was chosen to optimize the agreement between observed and calculated mean bond distances for all samples studied.

The eight equations are as follows:

$$26\text{Fe1} + 12\text{Mg1} = e^{-}\text{M1}_{obs} - 25\text{Mn} - 3\text{Li} \quad (1)$$

$$26\text{Fe2} + 12\text{Mg2} = e^{-}\text{M2}_{obs} - (13^{[6]}\text{Al} + 26\text{Fe}^{3+} + 22^{[6]}\text{Ti} + 24\text{Cr})/2 \quad (2)$$

$$\text{Fe1} + 2\text{Fe2} = \text{Fe}^{2+}_{tot} \quad (3)$$

$$\text{Mg1} + 2\text{Mg2} = \text{Mg}_{tot} \quad (4)$$

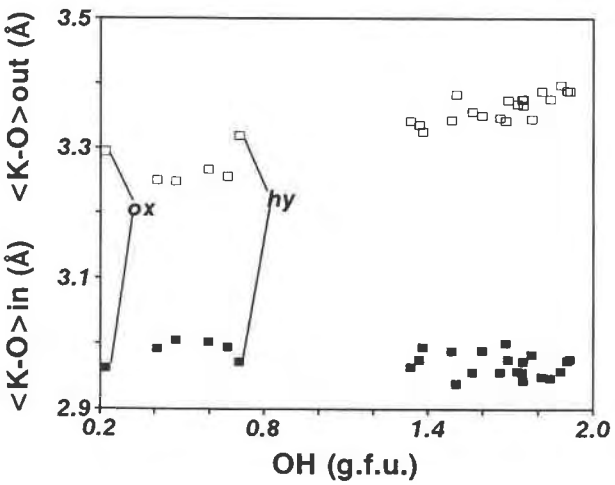

Fig. 3. Variations of longer ⟨K-O⟩ distance (open symbols) and shorter ⟨K-O⟩ distance (solid symbols) vs. OH content from formula calculation. Samples labeled ox and hy refer, respectively, to the oxybiotite of Ohta et al. (1982) and the hydrogenated oxybiotite of Takeda and Ross (1975).

$$\text{Fe1} + \text{Mg1} = 1 - \text{Mn} - \text{Li} - {}^{[6]}\square \quad (5)$$

$$\text{Fe2} + \text{Mg2} = 1 - ({}^{[6]}\text{Al} + \text{Fe}^{3+} + {}^{[6]}\text{Ti} + \text{Cr})/2 \quad (6)$$

$$\langle \text{Fe}^{2+}\text{-O}\rangle\text{Fe1} + \langle \text{Mg-O}\rangle\text{Mg1} = \langle \text{M1-O}\rangle_{obs} - \langle \text{Mn-O}\rangle\text{Mn} - \langle \text{Li-O}\rangle\text{Li} - \langle \square\text{-O}\rangle\square \quad (7)$$

$$\langle \text{Fe}^{2+}\text{-O}\rangle\text{Fe2} + \langle \text{Mg-O}\rangle\text{Mg2} = \langle \text{M2-O}\rangle_{obs} - (\langle \text{Al-O}\rangle^{[6]}\text{Al} - \langle \text{Fe}^{3+}\text{-O}\rangle\text{Fe}^{3+} + \langle \text{Ti-O}\rangle\text{Ti} - \langle \text{Cr-O}\rangle\text{Cr})/2 \quad (8)$$

where (1) Mg_{tot}, Fe_{tot}, [6]Ti, [6]Al, Fe^{3+}, Cr, Mn, Li are expressed as number of atoms per formula unit as calculated in Table 8; (2) [6]□ is calculated as (3 minus the sum of octahedral cations); (3) ⟨Mg-O⟩: 2.067, ⟨Fe^{3+}-O⟩: 2.053, ⟨Al-O⟩: 1.920, ⟨Ti-O⟩: 2.073, ⟨Cr-O⟩: 2.040, ⟨Fe^{2+}-O⟩: 2.11, ⟨Mn-O⟩: 2.014, ⟨Li-O⟩: 2.106, and ⟨□-O⟩: 2.21 Å are the "ideal" values for [6]M (or vacancy)–O average bond distances; (4) Fe1 and Fe2 are Fe^{2+} contents in M1 and M2; (5) Mg1 and Mg2 are Mg contents (atoms per site) in M1 and M2.

The results of the least-squares calculations are reported in Table 9.[1] Calculated and observed values for bond distances and electron densities show the best agreement compared with several other systems of equations based on various ordering schemes that we tried.

The comparison of the calculated Fe and Mg contents in M1 and M2 reveals overall enrichment of Fe^{2+} within M1 and a random distribution of Mg over the two octahedral sites (Fig. 7). Ordering of Fe^{2+} on M1 may be considered as an indirect consequence of partitioning of the high-charge, small-radius cations on M2, but it may also be favored by the greater distortion of the M1 coordination polyhedron. In fact, the strong differences in the crystal-field stabilization energy and covalency degree of bonds are known as acting as possible ordering factors

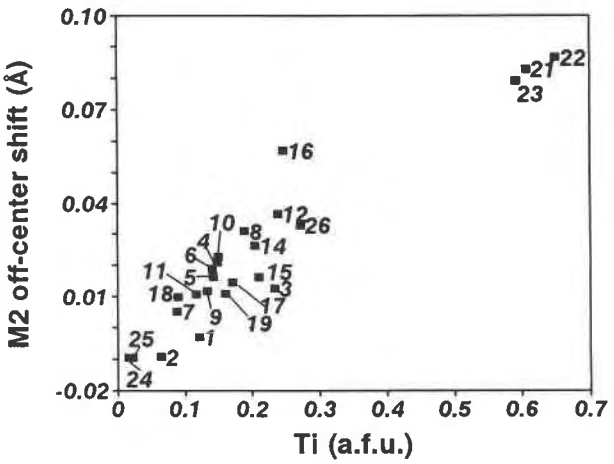

Fig. 5. Plot of the off-center shift of the cation within the M2 site vs. [6]Ti content: positive shifts are from the geometrical center toward the O4 sites, and negative shifts are toward the O3 sites.

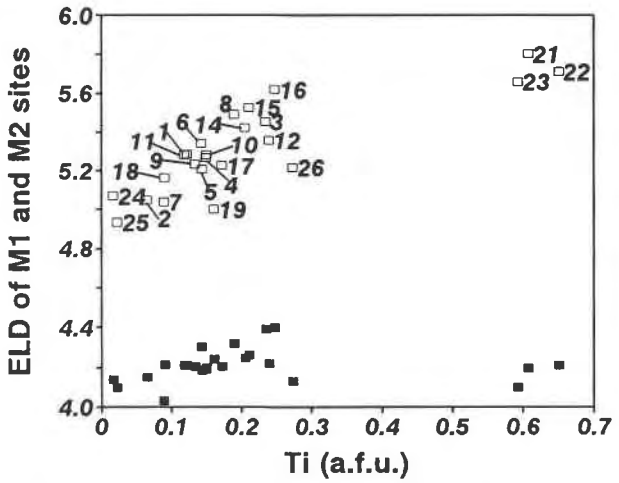

Fig. 6. Plot of edge-length distortion parameter of octahedral sites M1 (open symbols and labels) and M2 (solid symbols) vs. [6]Ti content.

of Mg and Fe^{2+} cations in ferromagnesian silicates. The general tendency of Fe^{2+} to be ordered into the trans M1 site of trioctahedral micas is better recognized in Fe-rich micas (cf. Brigatti and Davoli, 1990) in which electron densities on M2 are generally lower than those on M1. In Mg- and Ti-rich micas, the electron density at M2 is generally higher than that at M1, despite the enrichment of Fe in M1; this feature can be ascribed to partitioning of Ti into M2.

Bond valence and field strength calculations

A full description of the cation site population allows the determination of bond valences and mean field strengths.

The bond valences of each bond (s_{ij}) from the observed bond length distances (R_{ij}) were calculated by the equation $s_{ij} = \exp[R_{mix} - R_{ij})/0.37]$, by assuming as R_{mix} value the linear combination of the R_0 constants given by Brown and Altermatt (1985), weighted according to the composition of each site. Mixed occupancy (OH, F, O) was also approximately considered for bonds involving O4. The sums of bond valences for each site are reported in Table 10 and are in good agreement with the electrostatic balance requirements. In order to obtain the total charge at O4, the contribution of the H fraction should be added to the bond valence sum. The smallest value found for sample 3 agrees with its high F content, whereas the higher values for samples 21, 22, and 23 may be related to the shift of Ti toward O4 to compensate for the loss of the proton.

For Ti-rich samples, M2 bond valence sums are significantly lower than the average valence of the M2 cation obtained from its chemical composition. Still lower values are found if bond valence sums are calculated in the geometric center of the M2 polyhedron (see Table 10). In agreement with these observations, the off-center shift of Ti may be explained on the basis of the distortion theorem (Brown, 1992; Kunz and Armbruster, 1992), which derives from the concave shape of the correlation curve formed by the bond valence and bond lengths.

On the basis of this exponential curve, the increase in regularity of Ba-containing interlayer sites may also be explained. In fact, a net increase in positive charge on the interlayer central position, which is fixed by symmetry constraints, probably leads to a shortening of the $K\text{-}O_{outer}$ distances.

Mean field strengths (F.S.) (cf. Lin and Guggenheim, 1983) of the cation sites were calculated as the average of the valence to ionic radius ratios (from Shannon, 1976) weighted according to site population. Significant rela-

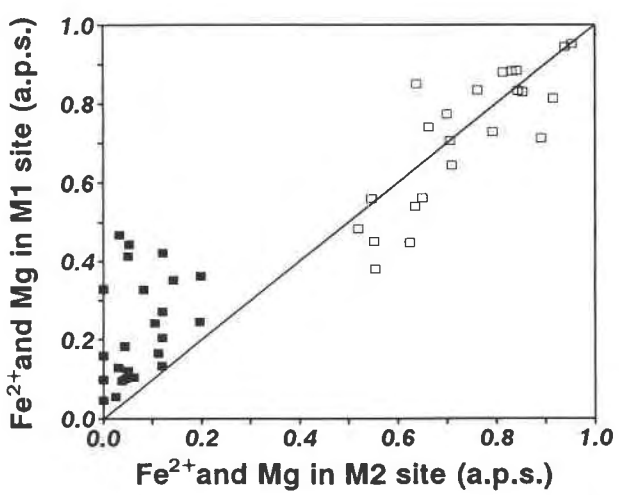

Fig. 7. Distribution of Fe (solid symbols) and Mg (open symbols) atoms per sites (a.p.s.) between M1 and M2 sites as determined from least-squares calculations.

TABLE 10. Bond valence sums for refined phlogopite

	1	2	3	4	5	6	7	8	9	10	11
K	0.81	0.84	0.84	0.85	0.83	0.84	0.83	0.84	0.82	0.87	0.84
T	3.72	3.71	3.82	3.71	3.71	3.74	3.71	3.78	3.71	3.72	3.69
M1	2.18	2.15	1.86	2.17	2.16	2.04	2.09	2.05	2.16	2.15	2.17
M2	2.22	2.17	1.92	2.24	2.23	2.08	2.17	2.21	2.24	2.24	2.23
O1	1.99	1.99	2.05	2.01	2.01	2.04	2.03	2.03	1.99	2.01	2.00
O1′	2.01	1.99	2.06	2.00	1.99	2.00	1.98	2.03	1.99	2.02	1.99
O2	1.99	1.97	2.05	2.00	2.00	2.00	1.98	2.05	1.98	2.00	1.99
O3	2.00	1.99	1.85	1.97	1.97	1.90	1.96	1.95	1.98	1.96	1.98
O4	1.17	1.15	1.06	1.23	1.21	1.16	1.15	1.21	1.20	1.23	1.20
$M2_{(val)}$	2.32	2.16	2.28	2.29	2.26	2.19	2.13	2.23	2.19	2.21	2.24
$M2_{cen}$	2.21	2.17	1.91	2.23	2.22	2.08	2.17	2.20	2.23	2.23	2.23

Note: values for each site are Σs_{ij}, $s_{ij} = \exp[(R_{mix} - R_{ij})/0.37]$ (Brown and Altermatt, 1985). $M2_{(val)}$: average valence of the M2 cation calculated from its chemical composition as $M2_{(val)} = \Sigma v_i m_i / \Sigma m_i$, where v_i = valence of *i*th cation and m_i = number of atoms per site of *i*th cation. $M2_{cen}$: bond valence sums calculated in the geometrical center of the M2 octahedron.

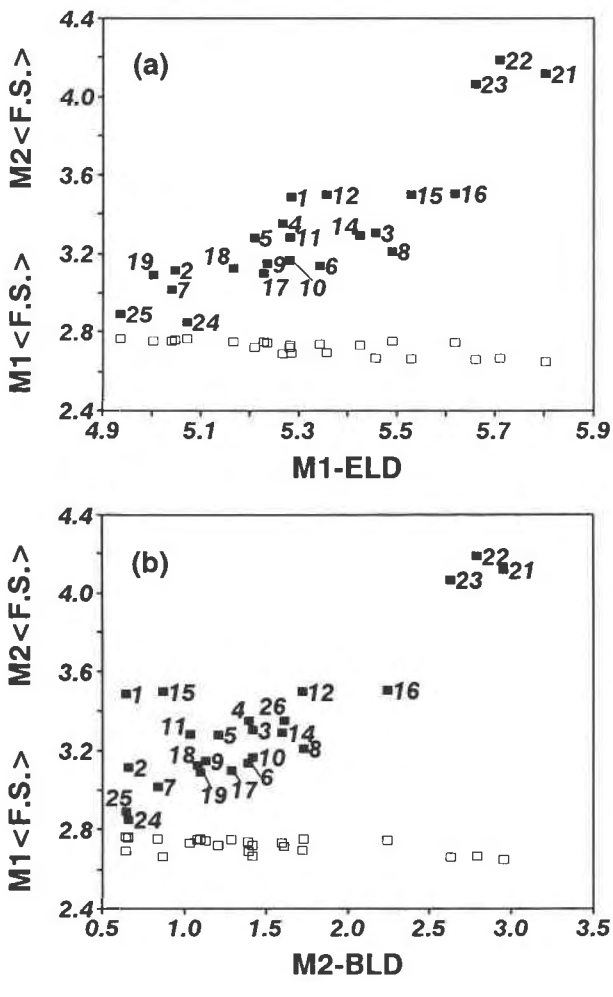

Fig. 8. (**a**) Variation of average field strengths (⟨F.S.⟩ of M1 sites (open symbols) and M2 sites (solid symbols and labels) vs. edge-length distortion of the M1 site (M1-ELD); (**b**) variation of average field strengths of M1 sites (open symbols) and M2 sites (solid symbols and labels) vs. bond-length distortion of the M2 site (M2-BLD).

tionships were found between the variation of $\langle F.S.\rangle_{M1}$ and $\langle F.S.\rangle_{M2}$ vs. the M1 and M2 distortion parameters. The external polyhedral distortion of M1 (M1-ELD) and the internal distortion of M2 (M2-BLD) increased strongly with $\langle F.S.\rangle_{M2}$ and decreased slightly with $\langle F.S.\rangle_{M1}$ (Fig. 8). These trends confirm the preference of the high-charge cations for M2.

SUBSTITUTION MECHANISMS IN PHLOGOPITE

This crystal chemical study may provide specific insights into some petrological aspects of micas. They mainly deal with the effects of Ti (as representative of high-charge, high-field elements) on the structure of mica, which is still poorly understood.

As shown, increased Ti content in phlogopite leads to the decrease of the *c* lattice parameter. Figure 9 shows that the shortening of $d_{(001)}$ is tightly linked to the decrease in K-O4 distances. The modifications of thickness associated to the three main mechanisms involved in Ti substitution in micas may be roughly estimated on the basis of the size differences in cations. For the substitution $^{[6]}R^{2+} + 2^{[4]}Si^{4+} = {}^{[6]}Ti^{4+} + 2^{[4]}Al^{3+}$ (Robert, 1976) a relatively small thinning of the octahedral sheet is expected from the replacement of Mg and Fe by Ti, whereas the replacement of Si^{4+} by Al^{3+} or Fe^{3+} should increase the tetrahedral thickness. In the substitution $2^{[6]}(R^{2+}) = {}^{[6]}(Ti^{4+}) + {}^{[6]}\square$ (Forbes and Fowler, 1974), the decrease of octahedral thickness due to the smaller radius of Ti is partially or completely compensated by the presence of the large vacancy. Only the substitution $^{[6]}(R^{2+}) + 2(OH)^- = {}^{[6]}(Ti^{4+}) + 2O^{2-}$ (Ti-oxy) implies shortening of the K-O4 distance because of the decreased interaction between the proton and the interlayer cation without effects on tetrahedral and octahedral sheet thicknesses. Moreover the off-center shift of Ti cations within M2 sites toward O4 is consistent with the loss of the proton bonded to O4. It follows that the Ti-oxy substitution mechanism best explains the observed structural adjustments. Evidence for the Ti-oxy substitution has also been recognized in amphiboles by means of single-crystal X-ray diffraction (Ob-

TABLE 10.—*Continued*

12	14	15	16	17	18	19	21	22	23	24	25	26
0.84	0.81	0.79	0.87	0.82	0.82	0.81	0.84	0.84	0.82	0.78	0.78	0.79
3.71	3.75	3.74	3.70	3.77	3.75	3.75	3.75	3.73	3.75	3.76	3.77	3.71
2.14	2.04	2.14	2.17	2.05	2.12	2.11	2.06	2.05	2.00	2.07	2.10	2.16
2.27	2.19	2.29	2.32	2.14	2.18	2.14	2.44	2.42	2.38	2.12	2.11	2.29
2.01	2.04	2.04	2.01	2.02	2.01	1.99	2.03	2.00	2.03	2.01	2.01	2.00
2.01	1.99	2.03	2.01	2.02	2.01	2.01	2.03	2.05	2.02	1.99	1.99	1.99
2.00	2.03	1.99	2.00	1.98	1.99	2.01	2.03	2.05	2.03	2.00	2.00	1.99
1.95	1.93	1.99	1.95	1.97	1.98	1.96	1.95	1.92	1.93	1.97	1.98	1.98
1.26	1.20	1.20	1.33	1.16	1.17	1.16	1.40	1.38	1.34	1.11	1.12	1.25
2.38	2.27	2.37	2.36	2.18	2.17	2.17	2.72	2.75	2.69	2.04	2.06	2.31
2.26	2.18	2.28	2.30	2.14	2.17	2.13	2.40	2.39	2.35	2.12	2.11	2.28

erti et al., 1992) and statistical analysis (Popp and Bryndzia, 1992). Dyar et al. (1993) recently showed that deficiencies in H^+ contents measured in common rock-forming hydroxyl silicate minerals (including a suite of metamorphic biotite) are most likely related to oxy-substitutions involving high-charge cations. From the above considerations we believe that, although neither Fe^{3+} nor OH^- concentrations has been determined for our samples, the structural analysis provides a reliable evaluation for the Ti-oxy substitution. The $(OH)^- \leftrightarrow O^{2-}$ exchange in micas is commonly neglected in formula calculations because of analytical uncertainties. This may be quite a satisfactory approximation when the TiO_2 content is low, but, when it rises, such an approximation can lead to serious errors in calculating the number of ions and thus the occupancies of the tetrahedral and octahedral sites. For instance, the OH^- contents of Ti-rich phlogopite from leucitites (samples 21, 22, 23) calculated by the relationship in Figure 1a is remarkably lower than the OH content estimated by the difference OH = 2 − F, suggesting the existence of a relatively large oxy-component. Formula calculation based on the assumption of 22 negative charges (i.e., neglecting the oxy-component) yields for these samples a considerable Al deficiency, in contrast to the observed tetrahedral bond lengths.

Implications for phlogopite stability

The higher thermal stability of phlogopite when F and Ti increases is well documented (Forbes and Flower, 1974; Foley, 1990; Peterson et al., 1991; Thibault et al., 1992). Synthesis experiments also show that the entry of Ti into Mg-rich micas is favored by increased f_{O_2} (Arima and Edgar, 1981; Foley, 1989) and by decreased H_2O activity (Tronnes et al., 1985; Foley, 1989). The structural and charge-balance requirements described for Ti substitution help us to understand these behaviors.

In general, as discussed from a geometric point of view by Hazen and Wones (1978) and Hazen and Finger (1982), in phlogopite with Si_3Al tetrahedral sheets the allowed range of tetrahedral rotation ($0° \leq \alpha \leq 12°$) imposes an upper limit to the octahedral sheet dimensions. The authors showed that micas containing large bivalent cations reach the geometrical limit $\alpha = 0°$ at temperature lower than micas with small-radius octahedral cations. In addition, a relatively small thermal expansion is expected for Ti^{4+}-containing octahedra, from its high ratio of valence to coordination number (Hazen and Prewitt, 1977). Furthermore, Toraya (1981) pointed out that the thermal

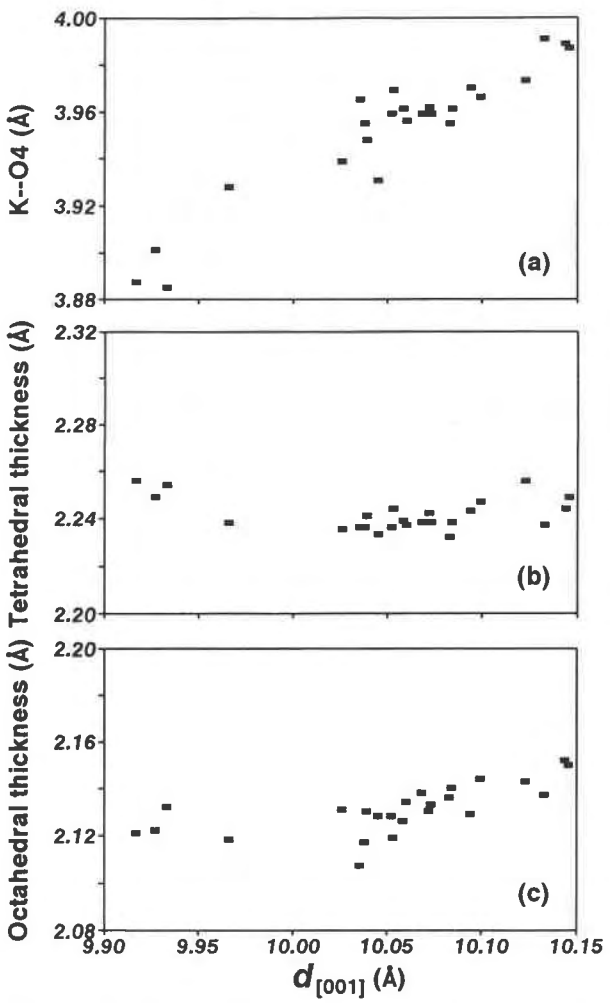

Fig. 9. Plot of $d_{[001]}$ vs. (a) K-O4 distance projected along **c***, (b) tetrahedral sheet thickness, (c) octahedral sheet thickness. Note the same range of variation on the vertical axes.

decomposition of octahedral layers in trioctahedral mica takes place along the chains of M2 sites, in agreement with the greater expansion rate of M2, as found from the high-temperature refinement by Takeda and Morosin (1975).

According to the above considerations, even low contents of $^{[6]}$Ti, partitioned into M2 sites, can increase remarkably the thermal stability of mica.

Several authors (Bol et al., 1989; Tracy, 1991, and references therein) described the occurrence of Ba and Ti-rich phlogopite in high-temperature metamorphic and igneous rocks. Our Ba- and Ti-rich phlogopite (samples 21, 22, 23) has small α (and $\Delta_{(K\text{-}O)}$) values. The enhanced regularity of the interlayer cavity may be ascribed to the loss of the proton at O4 resulting from the Ti-oxy substitution. This structural adjustment and the decreased repulsion should favor the entry of Ba in 12-fold coordination and results in a more homogeneous distribution of positive charge over the neighboring O atoms. Since thermal decomposition of mica may result from the breaking of the weak bonds between the anions around the interlayer cation (Takeda and Morosin, 1975), Ba substitution may also contribute to thermal stabilization of the whole structure.

Implications for mica-based geothermometric and geobarometric studies

Preferential partitioning of high-charge cations into M2 may have important consequences for the formulation of the biotite-garnet geothermometer. Multisite substitutions provide evidence of nonideality, which has to be considered in the mixing model for phlogopite-annite solid solutions (Guidotti and Dyar, 1991). In fact, even low contents of Ti may constrain both the polyhedral geometry of M2 and the distortion of M1, exerting a considerable degree of interference in the Fe-Mg intracrystalline ordering and the intercrystalline distribution between garnet and mica. Evidence of deviation from ideality arising from the occurrence of Ti and Al in the octahedral sites of biotite is well documented (Indares and Martignole, 1985; Dasgupta et al., 1991, and references therein).

Acknowledgments

The authors are grateful to the persons listed in Table 1 for providing samples. We would like to thank G.M. Molin for assistance at the electron microprobe facility of Centro per lo Studio dei Problemi dell'Orogeno delle Alpi Orientali (C.N.R., Padova) and L. Ottolini for the ion microprobe analysis at Centro per la Cristallografia e Cristallochimica (C.N.R., Pavia). We thank Martin Kunz and David A. Hewitt for their constructive reviews. Financial support was provided by C.N.R. and M.U.R.S.T. (grants to P.F.Z.). This research was part of the Ph.D. thesis by G.C., which was funded by M.U.R.S.T.

References cited

Abrecht, J., and Hewitt, D.A. (1988) Experimental evidence on the substitution of Ti in biotite. American Mineralogist, 73, 1275–1284.

Arima, M., and Edgar, A.D. (1981) Substitution mechanisms and solubility of titanium in phlogopites from rocks of probable mantle origin. Contributions to Mineralogy and Petrology, 77, 288–295.

Bailey, S.W. (1984) Crystal chemistry of true micas. In Mineralogical Society of America Reviews in Mineralogy, 13, 13–60.

——— (1988) X-ray diffraction identification of the polytypes of mica, serpentine, and chlorite. Clays and Clay Minerals, 36, 193–213.

Barker, D.S., and Nixon, P.H. (1989) High-Ca, low-alkali carbonatite volcanism at Fort Portal, Uganda. Contributions to Mineralogy and Petrology, 103, 166–177.

Bohlen, S.R., Peacor, D.R., and Essene, E.J. (1980) Crystal chemistry of a metamorphic biotite and its significance in water barometry. American Mineralogist, 65, 55–62.

Bol, L.C.G.M., Bos, A., Sauter, P.C.C., and Jansen, J.B.H. (1989) Barium-titanium-rich phlogopites in marble from Rogaland, southwest Norway. American Mineralogist, 74, 439–447.

Brigatti, M.F., and Davoli, P. (1990) Crystal-structure refinements of *1M* plutonic biotites. American Mineralogist, 75, 305–313.

Brigatti, M.F., Galli, E., Poppi, L. (1991) Effect of Ti substitution in biotite-*1M* crystal chemistry. American Mineralogist, 76, 1174–1183.

Brown, I.D. (1992) Chemical and steric constraints in inorganic solids. Acta Crystallographica, B48, 553–572.

Brown, I.D., and Altermatt, D. (1985) Bond-valence parameters obtained from a systematic analysis of the inorganic crystal structure database. Acta Crystallographica, B41, 244–247.

Conticelli, S., and Peccerillo, A. (1990) Petrological significance of high-pressure ultramafic xenoliths from ultrapotassic rocks of Central Italy. Lithos, 24, 305–322.

Cruciani, G. (1993) Comparative crystal chemical study on phlogopite-*1M*. Ph.D. thesis, University of Perugia, Italy (in Italian).

Cruciani, G., and Quartieri, S. (1992) XANES investigation on iron in phlogopite-*1M*: First results and perspectives. Proceedings of the Italian National School on Synchrotron Light and Chemical Research, Cagliari, 1–4.

Cruciani, G., and Zanazzi, P.F. (1992) Phlogopites from mantle derived rocks: Fe^{3+} in tetrahedral coordination. Proceedings of the Italian Association of Crystallography, L'Aquila, 114–115.

Cundari, A. (1973) Petrology of the leucite-bearing lavas in New South Wales. Journal of the Geological Society of Australia, 20, 465–492.

Cundari, A., and Ferguson, A.K. (1991) Petrogenetic relationships between melilitite and lamproite in the Roman Comagmatic Region: The lavas of S. Venanzo and Cupaello. Contributions to Mineralogy and Petrology, 107, 343–357.

da Silva, A.B., Marchetto, M., and de Souza, O.M. (1979) Geologia do complexo carbonatitico de Araxà (Barreiro), Minas Gerais. Mineraçao Metalurgia, 43 (415), 14–18.

Dasgupta, S., Sen Gupta, P.K., Guha, D., and Fukuoka, M. (1991) A refined garnet-biotite Fe-Mg exchange geothermometer and its application in amphibolites and granulites. Contributions to Mineralogy and Petrology, 109, 130–137.

Dyar, M.D., Guidotti, C.V., Holdaway, M.J., and Colucci, M. (1993) Nonstoichiometric hydrogen contents in common rock-forming hydroxyl silicates. Geochimica et Cosmochimica Acta, 57, 2913–2918.

Dymek, R.F. (1983) Titanium, aluminium and interlayer cation substitutions in biotite from high grade gneisses, West Greenland. American Mineralogist, 68, 880–899.

Foley, S.F. (1989) Experimental constraints on phlogopite chemistry in lamproites. I. The effect of water activity and oxygen fugacity. European Journal of Mineralogy, 1, 411–426.

——— (1990) Experimental constraints on phlogopite chemistry in lamproites. II. Effect of pressure-temperature variations. European Journal of Mineralogy, 2, 327–341.

Forbes, W.C., and Flower, M.F.J. (1974) Phase relations of titan-phlogopite, $K_2Mg_4TiAl_2Si_6O_{20}(OH)_4$: A refractory in the upper mantle? Earth and Planetary Science Letters, 22, 60–66.

Fraser, K.J., and Hawkesworth, C.J. (1992) The petrogenesis of group 2 ultrapotassic kimberlites from Finsch mine, South Africa. Lithos, 28, 327–345.

Fuster, J.M. (1956) Las erupciones delleniticas del Terciario superior de la fosa de Vera (provincia de Almeria). Boletín Real Sociedad Española de Historia Natural (Madrid), 54, 53–88.

Gervilla, F., and Leblanc, M. (1990) Magmatic ores in high-temperature Alpine-type lherzolite massifs (Ronda, Spain, and Beni Bousera, Morocco). Economic Geology, 85, 112–132.

Gianfagna, A., and Tuzi, F. (1988) Pyrrhotite-, diopside- and phlogopite-bearing "coronas" around olivine from the Albani Hills, Italy. Neues Jahrbuch für Mineralogie Monatshefte, 12, 529–538.

Giannetti, B., and Luhr, J.F. (1990) Phlogopite-clinopyroxenite nodules from high-K magmas, Roccamonfina Volcano, Italy: Evidence for a low-pressure metasomatic origin. Earth and Planetary Science Letters, 101, 404–424.

Geise, R.F., Jr. (1984) Electrostatic energy models of micas. In Mineralogical Society of America Reviews in Mineralogy, 13, 105–144.

Guggenheim, S. (1984) The brittle micas. In Mineralogical Society of America Reviews in Mineralogy, 13, 61–104.

Guggenheim, S., and Eggleton, R.A. (1987) Modulated 2:1 layer silicates: Review, systematics, and predictions. American Mineralogist, 72, 724–738.

Guggenheim, S., Chang, Y.-H., and Koster van Groos, A.F. (1987) Muscovite dehydroxylation: High-temperature studies. American Mineralogist, 72, 537–550.

Guidotti, C.V., and Dyar, M.D. (1991) Ferric iron in metamorphic biotite and its petrologic and crystallochemical implications. American Mineralogist, 76, 161–175.

Güven, N. (1971) The crystal structure of $2M_1$ phengite and $2M_1$ muscovite. Zeitschrift für Kristallographie, 134, 195–212.

Hazen, R.M., and Burnham, C.W. (1973) The crystal structure of one layer phlogopite and annite. American Mineralogist, 58, 889–900.

Hazen, R.M., and Finger, L.W. (1982) Comparative crystal chemistry, 231 p. Wiley, New York.

Hazen, R.M., and Prewitt, C.T. (1977) Effects of temperature and pressure on interatomic distances in oxygen-based minerals. American Mineralogist, 62, 309–315.

Hazen, R.M., and Wones, D.R. (1978) Predicted and observed compositional limits of trioctahedral micas. American Mineralogist, 63, 885–892.

Hewitt, D.A., and Abrecht, J. (1986) Limitations on the interpretation of biotite substitutions from chemical analyses of natural samples. American Mineralogist, 71, 1126–1128.

Holl, A. (1990) Geochemie von Lamproiten an aus südost-Jugoslawien. Ph.D. thesis, University of Karlsruhe, Germany.

Holl, A., and Altherr, R. (1991) Two generations of phlogopites in lamproites from south-eastern Yugoslavia. Terra Abstracts, 3, 24.

Ibers, J.A., and Hamilton, W.C., Eds. (1974) International tables for X-ray crystallography, vol. 4, 366 p. Kynoch, Birmingham, U.K.

Indares, A., and Martignole, J. (1985) Biotite-garnet geothermometry in the granulite facies: The influence of Ti and Al in biotite. American Mineralogist, 70, 272–278.

Keller, J., and Schleicher, H. (1990) Volcanism and petrology of the Kaiserstuhl. International Volcanological Congress, Mainz, Germany, Post-Conference Excursion 2B, 60 p.

Kunz, M., and Armbruster, T. (1992) Applications and limitations of the ionic potential model with empirically derived ion-specific repulsion parameters. Acta Crystallographica, B48, 553–572.

Kunz, M., Armbruster, T., Lager, G.A., Schultz, A.J., Goyette, R.J., Lottermoser, W., and Amthauer, G. (1991) Fe,Ti ordering and octahedral distortions in acentric neptunite: Temperature dependent X-ray and neutron structure refinements and Mössbauer spectroscopy. Physics and Chemistry of Minerals, 18, 199–213.

Lin, J.-C., and Guggenheim, S. (1983) The crystal structure of a Li,Be-rich brittle mica: A dioctahedral-trioctahedral intermediate. American Mineralogist, 68, 130–142.

Lombardo, B., Cappelli, B., Carmignani, L., Gosso, G., Memmi, I., Montrasio, A., Palmeri, R., Pannuti, F., Pertusati, P.C., Ricci, C.A., Salvini, F., and Talarico, F. (1987) The metamorphic rocks of the Wilson Terrane between David and Mariner Glaciers, North Victoria Land, Antarctica. Memorie della Società Geologica Italiana, 33, 99–130.

McCauley, J.W., and Newnham, R.E. (1971) Origin and prediction of ditrigonal distortions in micas. American Mineralogist, 56, 1626–1637.

McCauley, J.W., Newnham, R.E., and Gibbs, G.V. (1973) Crystal structure analysis of synthetic fluorophlogopite. American Mineralogist, 58, 249–254.

Munoz, J.L. (1984) F-OH and Cl-OH exchange in micas with applications to hydrothermal ore deposits. In Mineralogical Society of America Reviews in Mineralogy, 13, 469–493.

Newnham, R.E., and Brindley, G.W. (1956) The crystal structure of dickite. Acta Crystallographica, 9, 759–764.

Noda, T., and Ushio, M. (1965) Hydrothermal synthesis of fluorine-hydroxyl-phlogopites. II. Relationship between the fluorine content, lattice constants, and the conditions of synthesis of fluorine-hydroxyl-phlogopite. Geochemistry International, 1, 96–104.

North, A.C.T., Phillips, D.C., and Mathews, F.S. (1968) A semi-empirical method of absorption correction. Acta Crystallographica, A24, 351–359.

Oberti, R., Ungaretti, L., Cannillo, E., and Hawthorne, F.C. (1992) The behaviour of Ti in amphiboles. I. Four- and six-coordinate Ti in richterite. European Journal of Mineralogy, 4, 425–439.

Ohta, T., Takeda, H., and Takéuchi, Y. (1982) Mica polytypism: Similarities in the crystal structures of coexisting *1M* and $2M_1$ oxybiotite. American Mineralogist, 67, 298–310.

Peterson, J.W., Chacko, T., and Kuehner, S.M. (1991) The effects of fluorine on the vapor-absent melting of phlogopite + quartz: Implications for deep-crustal processes. American Mineralogist, 76, 470–476.

Popp, K.R., and Bryndzia, L.T. (1992) Statistical analysis of Fe^{3+}, Ti, and OH in kaersutite from alkalic igneous rocks and mafic mantle xenoliths. American Mineralogist, 77, 1250–1257.

Radoslovich, E.W. (1963) The cell dimensions and symmetry of layer-lattice silicates. IV. Interatomic forces. American Mineralogist, 48, 76–99.

Renner, B., and Lehmann, G. (1986) Correlation of angular and bond length distortions in TO_4 units in crystals. Zeitschrift für Kristallographie, 175, 43–59.

Robert, J.L. (1976) Titanium solubility in synthetic phlogopite solid solutions. Chemical Geology, 17, 213–227.

Shannon, R.D. (1976) Revised effective ionic radii and systematic studies of interatomic distances in halides and chalcogenides. Acta Crystallographica, A32, 751–767.

Sheldrick, G.M. (1976) SHELX76: Program for crystal structure determinations. University of Cambridge, Cambridge, U.K.

Stoppa, F., and Lavecchia, G. (1992) Late Pleistocene ultra-alkaline magmatic activity in the Umbria-Latium region (Italy): An overview. Journal of Volcanological and Geothermal Research, 52, 277–293.

Takeda, H., and Morosin, B. (1975) Comparison of observed and predicted structural parameters of mica at high temperature. Acta Crystallographica, B31, 2444–2452.

Takeda, H., and Ross, M. (1975) Mica polytypism: Dissimilarities in the crystal structure of coexisting *1M* and $2M_1$ biotite. American Mineralogist, 60, 1030–1040.

Thibault, Y., Edgar, A.D., and Lloyd, F.E. (1992) Experimental investigation of melts from a carbonated phlogopite lherzolite: Implications for metastomatism in the continental lithospheric mantle. American Mineralogist, 77, 784–794.

Toraya, H. (1981) Distortions of octahedra and octahedral sheets in *1M* micas and the relation to their stability. Zeitschrift für Kristallographie, 157, 173–190.

Tracy, R.J. (1991) Ba-rich micas from the Franklin Marble, Lime Crest and Sterling Hill, New Jersey. American Mineralogist, 76, 1683–1693.

Tronnes, R.G., Edgar, A.D., and Arima, M. (1985) A high pressure–high temperature study of TiO_2 solubility in Mg-rich phlogopite: Implications to phlogopite chemistry. Geochimica et Cosmochimica Acta, 49, 2323–2329.

Weiss, Z., Rieder, M., Chmielova, M., and Krajicek, J. (1985) Geometry of the octahedral coordination in micas: A review of refined structures. American Mineralogist, 70, 747–757.

Weiss, Z., Rieder, M., and Chmielova, M. (1992) Deformation of coordination polyhedra and their sheets in phyllosilicates. European Journal of Mineralogy, 4, 665–682.

Manuscript received April 12, 1993
Manuscript accepted November 12, 1993